568–574 *Nucleic Acids Research, 1997, Vol. 25, No. 3*

Evaluation of pyrimidine PNA binding to ssDNA targets from nonequilibrium melting experiments

Elena A. Lesnik*, Lisa M. Risen, David A. Driver[+], Michael C. Griffith[‡], Kelly Sprankle and Susan M. Freier

ISIS Pharmaceuticals, 2292 Faraday Avenue, Carlsbad, CA 92008, USA

Received October 7, 1996; Revised and Accepted December 5, 1996

ABSTRACT

Slow kinetics of homopyrimidine PNA binding to single stranded DNA and RNA targets is manifested in significant hysteresis in thermal UV absorption experiments. We have compared temperatures of dissociation (T_{dis}) and reassociation (T_{ass}) for triplexes formed by DNA and single or bis PNAs with K_{50} derived from gel mobility experiments. Results indicated there was no correlation between T_{dis} and K_{50} while reasonable correlation between T_{ass} and K_{50} was found. This correlation enabled use of easy thermal UV absorption experiments for evaluation of PNA binding to DNA/RNA targets.

INTRODUCTION

Some years ago, peptide-nucleic acid (PNA), a novel nuclease resistant DNA analog, was synthesized and described (1). Single homopyrimidine PNAs bind single stranded DNAs and RNAs in triplex fashion (2,3) while mixed purine-pyrimidine PNAs bind them in duplex fashion (4). UV melting experiments are a routine, fast, and convenient method for evaluation of oligonucleotide binding. However, slow kinetics of triplex formation reported for single homopyrimidine PNA binding are manifested in significant hysteresis for UV melting–cooling curves (5–8). The question arose whether we could use data derived from melting experiments for evaluation of oligonucleotide binding and if we could compare them with K_{50} derived from gel mobility or filter binding assays usually used for evaluation of slow binding processes (9–12).

In this paper, we compare K_{50} obtained from gel mobility assay and data obtained from dissociation and reassociation nonequilibrium thermal experiments for a set of pyrimidine PNAs binding single stranded DNA and RNA targets. No correlation was observed between temperature of triplex dissociation (T_{dis}) determined as the temperature of the main maximum in the first derivative of the dissociation (heating) curve and K_{50}. On the other hand, reasonable correlation between temperature of association (T_{ass}) determined as the temperature of the maximum in the first derivative of the reassociation (cooling) curve and K_{50} was found. The correlation enabled us to evaluate binding of the pyrimidine PNAs to single stranded targets using easy thermal experiments and to shed some light on the mechanism of triplex formation and stability.

MATERIALS AND METHODS

PNA and oligonucleotide synthesis

PNAs were synthesized and purified as described elsewhere (5) and were analyzed by high performance liquid chromatography (HPLC) and mass spectrometry. By analogy to peptides, PNA sequences are written from amino (N) to carboxy (C) terminus (4). Oligonucleotides were synthesized using an Applied Biosystems 380B automated DNA synthesizer and standard phosphoramidite chemistry (13).

Thermal melting–cooling experiments

Absorbance versus temperature curves were measured in a Gilford Response II spectrophotometer. Samples were prepared in the buffers indicated at 8 μM total strand concentration. The ratio of PNA to target (single stranded DNA or RNA) was 2:1 for single pyrimidine PNAs and 1:1 for bis PNAs. Prior to each experiment, samples were heated at 90–95°C for 15 min and then incubated at room temperature for 2 h. Unless otherwise indicated, absorbance at 260 nm was measured as a function of temperature as samples were heated from 15 to 98°C at 0.7°C/min. After 10 min incubation at 98°C, samples were cooled at the same rate. Reported temperatures for T_{dis} and T_{ass} are the maxima in the first derivatives [dA(260)/dT] for heating and cooling respectively. Reported halfwidth of the peaks in first derivative curves were measured at half height of the peaks. Reproducibility in peak position was ±0.5°C. Pattern of 'minor' peaks were reproducible for melts performed under identical conditions.

Gel mobility assays

PNA binding was measured using a gel mobility assay (11). Radiolabeled target (~10 pM DNA or RNA) was incubated with increasing concentrations of PNA at 37°C for 20–24 h in 100 mM Na^+, 10 mM phosphate buffer (pH 7.0), 0.1 mM EDTA. An

* To whom correspondence should be addressed. Tel: +1 619 603 2377; Fax: +1 619 931 0209; Email: elesnik@isisph.com

Present addresses: [+]Chiron Viagene, 11055 Roselle Street, San Diego, CA 92121, USA and [‡]Houghten Pharmaceuticals, 3550 General Atomic Court, San Diego, CA 92121, USA

increase in incubation time did not result in a decrease of K_{50} values suggesting equilibrium was reached within 20 h (data not shown). Reactions were resolved at 4°C in a 12% native polyacrylamide gel containing 44 mM tris-borate, 1 mM $MgCl_2$. We define K_{50} as the PNA concentration at which 50% of the target is bound (11).

RESULTS

Single stranded pyrimidine PNAs with and without positively charged *lysines* at the C-terminus and bis pyrimidine PNAs were evaluated for hybridization to DNA and RNA targets (see Table 1 for a list of sequences studied). Pyrimidine PNAs hybridize to single stranded DNA and RNA targets in triplex fashion and can bind them in two orientations: parallel (N-terminus of PNA binds to 5′-end of DNA/RNA target) and antiparallel (N-terminus of PNA binds to 3′-end of DNA/RNA target) (3,14). We synthesized both parallel and antiparallel targets for each PNA (Table 1). Mixed purine-pyrimidine PNA 11 was included in the study to compare the pH effect on duplex and triplex formation. PNAs 2, 3 and bis-PNAs 8 and 9 had the same base sequence but differed in the presence of *lysine* and the direction of sequence from N to C terminus (PNAs 2 and 3) or in the chemistry of linkers in bis-PNAs 8 and 9. PNAs 5 and 6 had the same base sequence oriented in opposite directions from N to C terminus. PNA 7 and bis PNA 10 had the same symmetrical base sequence and therefore one DNA target (22, Table 1) was synthesized for them. Thus, we had five different base sequences arranged differently in ten PNAs to test the effect of PNA structure peculiarities on K_{50} and UV-melting data.

Table 1. PNA and corresponding parallel and antiparallel target sequences used in the studies

#	PNA sequences	C-content (%)
Single PNAs without -lys$^+$		
1	H-gly-CCTCCTTCCC-NH_2[a]	70
2	H-gly-TTCTCTCTCT-NH_2	40
Single PNAs with -lys$^+$		
3	H-gly-TCTCTCTCTT-_lys$^+$-NH_2	40
4	H-gly-TTTTCCCTTCCTTTT-_lys$^+$-NH_2	33
5	H-gly-TCTCCCTCTCCTTTT-_lys$^+$-NH_2	47
6	H-gly-TTTTCCTCTCCCTCT-_lys$^+$-NH_2	47
7	H-gly-TTTTCTTTT-_lys$^+$-NH_2	11
Bis PNAs with -lys$^+$		
8	H-gly-TTCTCTCTCT-(3PEG-3PEG)-TCTCTCTCTT-_lys$^+$ - NH_2 [b]	40
9	H-gly-TTCTCTCTCT-(lys$^+$-Aha)$_2$-lys$^+$-TCTCTCTCTT-_lys$^+$ - NH_2 [b]	40
10	H-gly-TTTTCTTTT-(lys$^+$-Aha)$_2$-lys$^+$-TTTTC TTTT-_lys$^+$ - NH_2	11
Mixed purine–pyrimidine PNA		
11	H-gly-TAATGCCTACCATATGC-_lys$^+$-NH_2	29
#	DNA target sequences	Direction
Targets to single PNAs without -lys$^+$		
12	5′-dGGAGGAAGGG	parallel to 1
13	5′-dGGGAAGGAGG	antipar. to 1
14	5′-dAAGAGAGAGA	parallel to 2
15	5′-dAGAGAGAGAA	antipar. to 2
Targets to single PNAs with -lys$^+$		
16	5′-dATTGT**AGAGAGAGAA**T [c]	parallel to 3
17	5′-dT**AAGAGAGAGA**TGTTA	antipar to 3
18	5′-d**AAAAGGGAAGGAAAA**GG	parallel to 4
19	5′-dGG**AAAAGGAAGGGAAAA**	antipar. to 4
20	5′-dAGAGGGAGAGGAAAA	parallel to 5 antipar. to 6
21	5′-dAAAAGGAGAGGGAGA	antipar. to 5, parallel to 6
22	5′-dATTGT**AAAAGAAAA**TGTTA	parallel and antipar. to 7 and 10 (bis)
Targets to bis PNAs with -lys$^+$		
23	5′-dATTGT**AGAGAGAGAA**T	parallel and antipar. to 8 and 9
24	5′-rATTGT**AGAGAGAGAA**T	RNA version of 23
Targets to mixed purine-pyrimidine PNA		
25	5′-dAATACGCATGGTATACG	parallel to 11
26	5′-dCGATATGGTACGCATTA	antipar. to 11

[a]PNA base sequences are written from N to C terminus. PNA structures are shown in (25).
[b]bis PNA linkers: 3PEG designates $H_2N(CH_2CH_2O)_3CH_2COOH$ and Aha designates 6-aminohexanoic acid.
[c]Bold letters denote the target sequence if it consists of only a part of the oligonucleotide.

Dissociation curves for single pyrimidine PNA_2–DNA triplexes

Examples of dissociation (heating) curves are presented in Figure 1 (plots a, b, e, f, i, and j). For two triplexes with antiparallel PNA orientation to DNA (PNAs 4 and 6), we observed only one transition in the dissociation curves (e.g. Fig. 1f). For all other triplexes with single PNAs, dissociation curves exhibited more than one transition. Comparison of the melting curves indicated the different orientation of the same PNA toward DNA target resulted in different patterns of 'minor' peaks while 'main' high temperature peaks in the differential melting curves remained similar. Preincubation of PNA/DNA mixtures from 1 h to 3 days at 20°C or 37°C resulted in some changes in size, shape, and positions of minor peaks but no changes were observed for the main peaks (data not shown).

Reassociation curves for single PNA_2–DNA triplexes

In contrast to dissociation curves, reassociation (cooling) curves always exhibited a single cooperative transition manifested as one peak in the first derivative plot (Fig. 1c, d, g, h, k, l). For most PNA complexes, the maximum in the reassociation curve was at a lower temperature than the 'minor' peaks in the dissociation curve. Hysteresis between main peaks in the dissociation and reassociation curves ranged from 8 to 36°C. The halfwidths of reassociation transitions were 6–8°C compared to 5–7°C for equilibrium dissociation–reassociation curves of similar length oligonucleotide duplexes.

Dissociation and reassociation curves for bis PNAs

Bis PNAs form triplexes with single stranded DNA and RNA targets binding them in 1:1 ratio with each 'arm' of the bis PNA binding in opposite orientation (5,8). Hybridization rates for bis PNAs are reported to be faster than for single PNAs (8). The hysteresis observed for bis PNAs 8–10 (Table 1) was reduced 3–30 times compared to single PNAs depending on PNA base composition, linker chemistry, and target. Bis PNA 10 comprising 11% cytosines in each arm and three positively charged *lysines* in the linker exhibited very cooperative transitions with high T_{dis} and T_{ass} values and negligible hysteresis (Fig. 2a). In contrast, bis PNA 8 with 40% cytosines and neutral poly(ethylene glycol) linker exhibited broad transitions and almost 10°C hysteresis (Fig. 2b).

Effect of acidic pH on PNA_2–DNA triplex dissociation and reassociation curves

Protonation of PNA cytosines at pH 5.5 shifted both the major and minor peaks in the dissociation curves to higher temperatures (compare Fig. 1a, b and Fig. 3a, b). Moreover, for PNA 1 and 2 without *lysine* at the C terminus, the size of the lower temperature peak became equal or even larger than the higher temperature peak (Fig. 3a, b). Association curves at pH 5.5 revealed a single cooperative transition similar to that observed in neutral solution (Fig. 3c, d). T_{ass} for three PNAs with parallel and antiparallel DNA targets measured at pH 7.0 and 5.5 are listed in Table 2. T_{ass} increased by 4.5–17.5°C in acidic solution compared to that at neutral pH. At pH 5.5, T_{ass} for triplexes with PNAs 2, 4, and 5 were similar at both PNA orientations whereas at pH 7.0, T_{ass} for triplexes 4 and 5 depended on PNA orientation. PNA 11 with mixed purine-pyrimidine base composition was used as a control demonstrating cytosine protonation resulted in insignificant decrease of T_{ass} for PNA–DNA duplex formation.

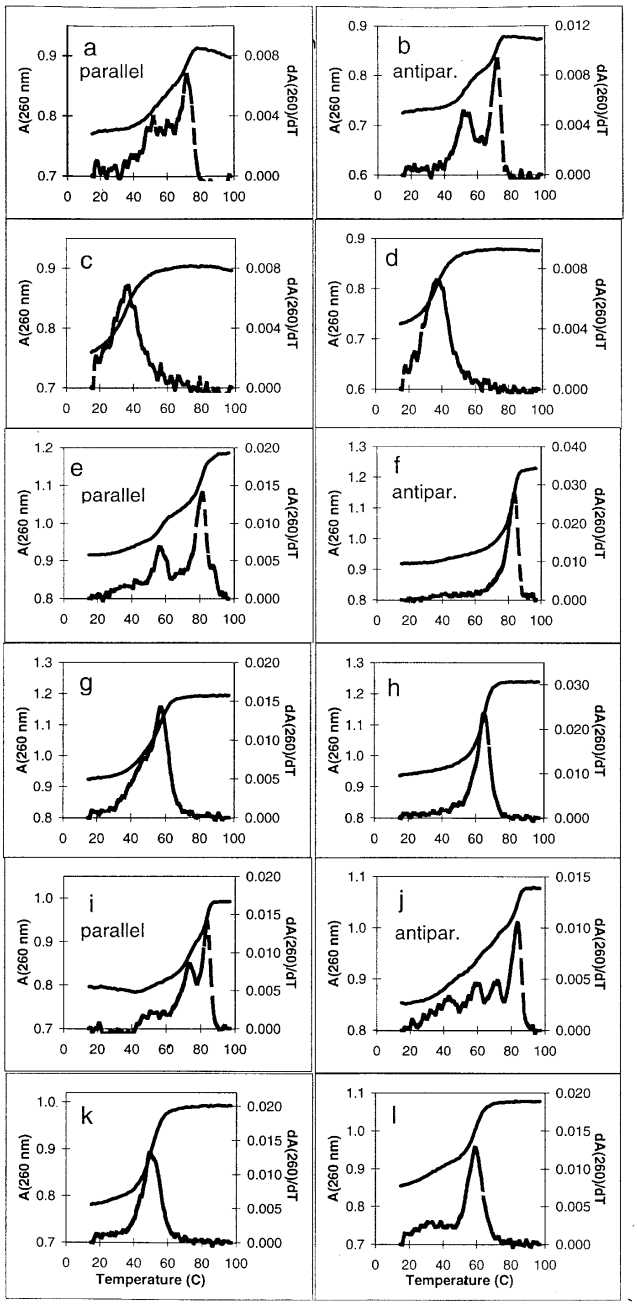

Figure 1. Thermal integral (—) and first derivative (----) curves for dissociation (**a**, **b**, **e**, **f**, **i**, and **j**) and reassociation (**c**, **d**, **g**, **h**, **k**, and **l**) of PNA_2–DNA triplexes formed by DNA targets and PNA 2 (a–d); PNA 4 (e–h); and PNA 5 (i–l) in 100 mM Na^+, 10 mM phosphate buffer (pH 7.0), 0.1 mM EDTA. (The orientations of DNA targets versus PNAs are indicated in plots.)

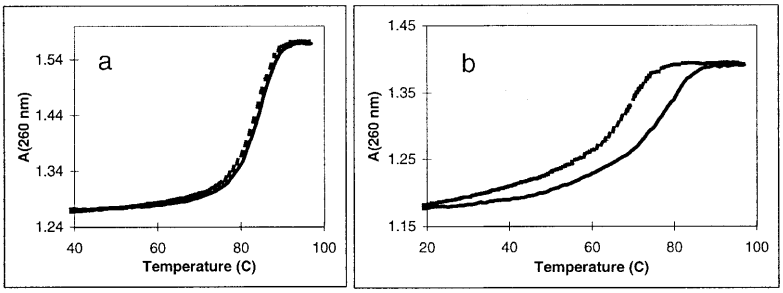

Figure 2. Dissociation (—) and reassociation (----) curves for bis PNA–DNA triplexes in 100 mM Na^+, 10 mM phosphate buffer (pH 7.0), 0.1 mM EDTA for PNA10 (**a**) and PNA 8 (**b**).

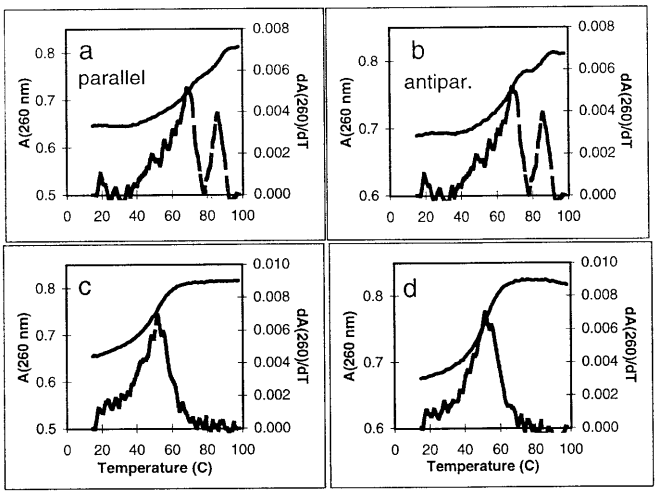

Figure 3. Thermal integral (—) and first derivative (----) curves for dissociation (**a**, **b**) and reassociation (**c**, **d**) of PNA_2–DNA triplexes formed by DNAs and PNA 2 in 100 mM Na^+, 10 mM cacodilate buffer (pH 5.5), 0.1 mM EDTA. The orientations of DNA targets versus PNA are indicated in plots.

Table 2. Temperatures of reassociation (T_{ass}) for PNA_2–DNA triplexes in neutral (10 mM cacodilate buffer, pH 7.0) and acidic (10 mM cacodilate buffer, pH 5.5) buffers containing 100 mM Na^+ and 0.1 mM EDTA.

#	Both PNA strands parallel to target				Both PNA strands antiparallel to target			
	T_{ass} pH 7.0	T_{ass} pH 5.5	ΔT^a (5.5–7.0)	$\Delta T/C^{+a}$	T_{ass} pH 7.0	T_{ass} pH 5.5	ΔT (5.5–7.0)	$\Delta T/C^+$
2	36.2	52.2	16.0	4.0	37.8	52.2	14.4	3.6
4	57.3	68.3	11.0	2.2	64.8	69.3	4.5	0.9
5	49.8	67.3	17.5	2.5	59.2	68.2	9.0	1.3
11	57.8	56.8	–1.0	–0.02	75.3	73.3	–2.0	–0.04

[a]ΔT is the difference between T_{ass} measured at pH 5.5 and 7.0; $\Delta T/C^+$ is ΔT per cytosine residues in Hoogsteen PNA strand

K_{50} values for pyrimidine PNA binding to single stranded targets

K_{50} was measured for each PNA listed in Table 1. K_{50} values varied from 30 pM up to 300 nM demonstrating a wide range of PNA affinity to the targets (Table 3). It should be noted that at high PNA concentration, the major shifted band in the polyacrylamide gel was sometimes accompanied by one or a few minor bands of slower mobility suggesting formation of more than one type of complex.

Comparison of dissociation constants (K_{50}) and T_{ass} and T_{dis}

All T_{dis} and T_{ass} values derived from melting–cooling curves and K_{50} values derived from gel shift mobility experiments are compiled in Table 3. For all PNAs (except case 9′), T_{ass} was lower than T_{dis} and no other correlation between T_{dis} and T_{ass} was observed. For some PNAs, a small difference in T_{ass} corresponded to a big difference in T_{dis} (e.g. PNAs 1 and 2 versus parallel targets or PNAs 6+5 and PNA 6 versus antiparallel target). For some others, a small difference in T_{dis} corresponded to a big difference in T_{ass} (e.g. PNA 6 versus parallel target and bis PNA 9 versus DNA target). The most important observation was that similar T_{dis} values corresponded to K_{50} values differing from each other as much as 10–20-fold. Thus two parameters routinely used to characterize the affinity of the oligonucleotides and their analogs to DNA/RNA targets did not correlate with each other. On the other hand, decrease in K_{50} correlated well with increase in T_{ass} values. Realizing this, we plotted T_{ass} versus log K_{50} for all PNA–DNA complexes studied (Fig. 4a) to find out whether the T_{ass} quantitatively correlated with K_{50}'s and could be used for the PNA affinity evaluation. Comparison of the two plots in Figure 4 demonstrated there was a reasonable correlation between T_{ass} and K_{50} (Fig. 4a) while no correlation between T_{dis} and K_{50} values was observed (Fig. 4b). All T_{ass} values for single PNAs fell on a single line. Points corresponding to bis PNAs in four of five cases fell higher than the correlation predicted and we discuss this below.

DISCUSSION

Relationship between T_{ass} and K_{50}

Developed for measurement of slow protein–nucleic acid binding (15,16), electrophoretic shift mobility assays are also successfully used now for evaluation of slow complex formation between structured DNA, RNA and oligonucleotides or analogs (9,11,12). However, gel mobility shift assay is time and labor intensive and quantitative reproducibility is limited (9). Measurement of dissociation and reassociation curves by UV absorption spectroscopy is a rapid, easy, and reproducible technique for determination of complex formation if it occurs under equilibrium conditions. Under nonequilibrium conditions, temperatures of dissociation and reassociation depend on the heating rate (17).

Table 3. Temperatures of Triplex Dissociation (T_{dis}) and Reassociation (T_{ass}) and K_{50} values for PNAs binding DNA targets in 10 mM phosphate buffer (pH 7.0), 100 mM Na^+, 0.1 mM EDTA

PNA[a]	Both PNA strands parallel to target				Both PNA strands antiparallel to target				PNA strands parallel and antiparallel to target			
	T_{dis}	T_{ass}	Δ[b]	K_{50} (nM)	T_{dis}	T_{ass}	D	K_{50} (nM)	T_{dis}	T_{ass}	Δ[a]	K_{50} (nM)
1	47.8	36.8	–11.0	300	40.0	39.8	–0.2	–				
2	72.2	36.2	–36.0	125	71.2	37.8	–33.4	150				
3	83.2	47.7	–35.5	12.0	82.8	50.3	–28.5	20.0				
4	81.0	57.3	–23.7	0.4	83.7	64.8	–18.9	0.7				
5	84.1	49.8	–34.3	9.3	83.7	59.2	–24.5	1.2				
6	85.7	49.8	–35.9	12.0	69.7	61.2	–8.5	0.8				
5+6*									93.6	63.2	–30.4	0.4
6+5*									96.0	61.2	–34.8	0.6
7*									74.7	47.9	–26.8	9.0
8									80.8	69.8	–11.0	0.2
9									85.2	76.3	–8.9	0.3
9′									82.8	82.8	0	0.3
9*									92.8	87.8	4.0	0.03
10									85.2	84.3	–0.9	0.16

[a]PNA numbers in Table 1.
[b]$\Delta = T_{ass} - T_{dis}$ is hysteresis between dissociation and reassociation curves.
5+6*, PNA 5 bound DNA target in parallel direction and PNA (6) bound target in antiparallel direction;
6+5*, PNA 6 bound DNA target in parallel direction and PNA (5) bound target in antiparallel direction;
7*, PNA 7 has symmetrical base sequence and can bind the same target in both orientation
9′, T_{dis} and T_{ass} were obtained in melting-cooling experiment with heating rate 0.1°C/min.
9*, PNA 9 bound RNA target.

Hysteresis of 25–30°C has been reported for PNA triplexes heated and cooled at rates of 0.1 and 1°C/min (5–7). At a rate 0.7°C/min, we observed hysteresis of 8–36°C for triplexes with single PNAs and 1–10°C for triplexes with bis PNAs depending mainly on cytosine content in the PNA strands and linker chemistry. Decrease of the heating/cooling rate down to 0.2°C/min resulted in an increase of T_{ass} by 1–3°C and in a decrease of T_{dis} by 3–7°C (measured for four triplexes). A temperature rate of 0.1°C/min reduced hysteresis even more but did not eliminate it for triplexes with single PNAs (data not shown) indicating the characteristic time of experiments was still much lower than the relaxation time of triplex dissociation and reassociation at equilibrium (18). Therefore, we cannot reach equilibrium in routine UV experiments and thus, cannot evaluate true PNA affinity directly from melting curves (7). In contrast to T_{dis} and T_{ass}, K_{50} values obtained under equilibrium conditions reflect genuine PNA affinities. The observation of a correlation between K_{50} and T_{ass} values enabled us to use simple and rapid UV spectroscopy method for evaluation of PNA affinity to single stranded DNA/RNA targets.

The observed results lead to some questions. The first question addressed was why the shape of dissociation and reassociation curves in general were so different. The second question was why T_{ass} but not T_{dis} correlated with K_{50} . The proposed model of triplex formation confirmed by CD titration data (3) suggests the duplex–triplex equilibrium strongly favors triplex formation (Scheme 1):

$$\mathrm{DNA} + 2\mathrm{PNA} \underset{k_{-1}}{\overset{k_{+1}}{\Leftrightarrow}} \mathrm{DNA{-}PNA} + \mathrm{PNA} \underset{k_{-2}}{\overset{k_{+2}}{\Leftrightarrow}} \mathrm{DNA{-}PNA_2} \qquad (1)$$

The kinetic model of PNA invasion in a DNA duplex also assumes the triplex formation occurs only if the PNA–DNA duplex is immediately trapped by a second PNA strand (19). Cooperativity of the association curves and the location of their first derivative peaks (T_{ass}) at temperatures lower than those for most peaks in the dissociation curves (Fig. 1) suggest that under cooling at a rate 0.1–0.7°C/min, PNA–DNA association occurred in a temperature range where triplex was much more stable than duplex and therefore the duplex concentration was insignificant. The dissociation curves usually exhibited more than one transition suggesting the minor peaks corresponded to the triplex to duplex dissociation and the major peak (T_{dis}) reflected in most cases the duplex dissociation. All data reported are consistent with the proposed triplex formation mechanism (3) if $k_{-1} \cong k_{-2}$ and $k_{+2} >> k_{+1}$ (Scheme 1). This consideration helps to understand why T_{ass} reflecting the nonequilibrium concentration of triplex and single strands correlated with K_{50} which measures equilibrium concentration of the same species in solution.

The next question addressed was how the transition from nonequilibrium to true equilibrium conditions would affect the correlation shown in Figure 4a. Data obtained for bis PNA–DNA triplexes answered this question. Formation and dissociation of triplexes with bis-PNAs occurred nearer to equilibrium than those for triplexes with single PNAs (5,8). The hysteresis for bis

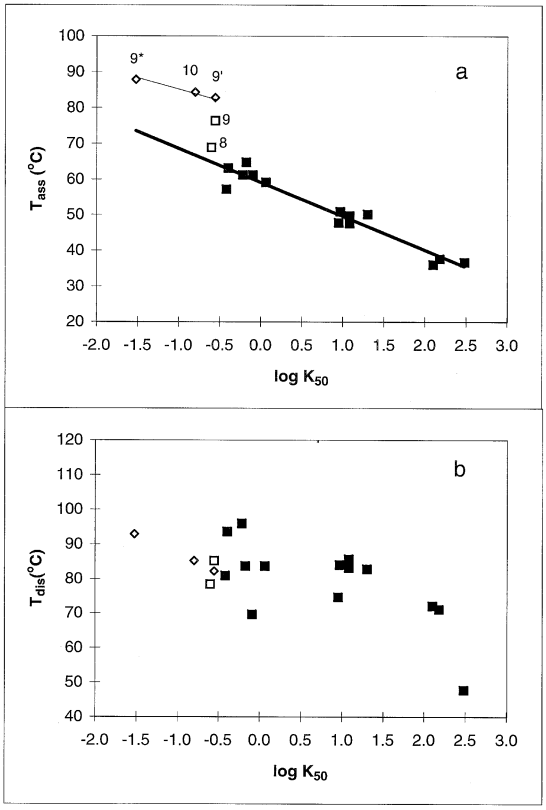

Figure 4. Relationships between K_{50} and T_{ass} (**a**) or T_{dis} (**b**) for heating and cooling of triplexes formed by single PNAs and DNA targets(■); triplexes formed by bis PNAs and DNA/RNA targets with low hysteresis between dissociation and reassociation curves (◇); for triplexes formed by bis PNA 8, 9 and DNA target with moderate hysteresis between dissociation and reassociation curves (□). (The solid line was drawn through data for single PNAs. The broken line was drown through points corresponding to bis PNAs in cases 9′, 9*, and 10 in Table 3.)

PNA–DNA triplexes heated and cooled with the rate 0.7°C/min was only 1°C if the triplex contained 11% C-G-C triplets (PNA 10, Table 3), 9–10°C for triplexes with 40% C-G-C triplets (PNAs 8 and 9, Table 3), and 4°C if bis PNA 9 bound RNA target (9*, Table 3). The decrease of temperature rate down to 0.1°C/min resulted in elimination of hysteresis for triplex of bis PNA 9 with DNA (9′, Table 3). The data in Figure 4a demonstrate the closer the dissociation–reassociation process was to equilibrium the more T_{ass} laid above the line for single PNAs. A line can be drawn through these points parallel to the former one. In contrast to bis PNAs 9 and 10 with positively charged *lysines* in linkers, bis PNA 8 having neutral PEG-containing linker displayed lower T_{ass} than its counterpart bis PNA 9 and much wider transitions than both *lysine* containing bis PNAs 9 and 10 indicating significant effect of linker chemistry on kinetics and stabilization. In Figure 4a, the point corresponding to PNA 8 fell close to those for single PNAs whereas the point corresponding to its counterpart PNA 9 lay closer to the upper line for bis PNAs. Thus, the data indicated the shift from nonequilibrium to equilibrium processes resulted in an upward shift of the straight line correlation.

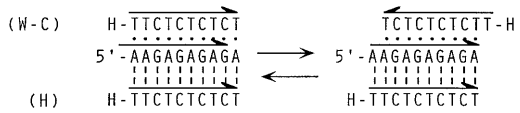

Figure 5. The possible structure for alternative complexes of PNA 2 with the parallel DNA target 14 (Table 1).

Effect of PNA orientation on PNA binding

Using the correlation obtained we tried to evaluate the effect of PNA orientation and cytosine protonation on PNA binding. The data in Table 3 indicated there was no preferential orientation of PNA 2 and 3 to DNA targets while for PNAs 4, 5, and 6, antiparallel binding to complementary DNA was preferred. Simultaneous parallel and antiparallel PNA binding to the same target (5+6 and 6+5 triplexes in Table 3) resulted in a very small decrease in K_{50} and increase in T_{ass} compared to antiparallel binding of both PNA strands. This observation correlates with molecular mechanics calculations (20) and conformational analysis data (21) predicting a small gain in triplex stabilization when the Watson–Crick (W–C) and Hoogsteen (H) PNA strands are antiparallel to each other. PNA 1 with 70% cytosines apparently formed a triplex with the parallel DNA target as indicated by the bi-phasic dissociation and 11°C hysteresis (1, Table 3). A monophasic dissociation curve (data not shown) and lack of hysteresis for the complex of PNA 1 with antiparallel DNA target (Table 3) suggests only a PNA–DNA duplex formed at pH 7.0. The gel shift assay indicated that K_{50} for PNA 1 binding antiparallel DNA target at 37°C was weaker than 10 µM.

The reported X-ray structure of a pyrimidine bis PNA–DNA triplex (22) suggests a strong Van der Waals interaction and hydrogen bonding between DNA and H-PNA backbones. These data explain enhanced affinity of H-PNA strand with moderate cytosine content compared to affinity of Hoogsteen oligonucleotide strands in DNA triplexes at pH 7.0 (23,24). Moreover, the X-ray data indicate that W–C PNA strand of bis PNA is antiparallel to DNA target suggesting this is preferable orientation for W–C PNA strand in both duplex and triplex PNA–DNA structures (22). Based on this suggestion, we can speculate that extra minor peaks in dissociation curves reflected melting out of complexes with alternative mismatched or shifted structures including complexes with reversed binding of W–C PNA strands to parallel DNA targets as shown in Figure 5.

Effect of cytosine protonation

At pH 5.5, protonation of cytosines results in additional electrostatic attraction and Hoogsteen G-C^+ hydrogen bond formation between H-PNA and DNA target. The change of pH from 7.0 to 5.5 resulted in a small decrease of T_{ass} for mixed purine-pyrimidine PNA 11 (Table 2) which forms a PNA–DNA duplex with only W–C hydrogen bonds (4). Therefore protonation of the Hoogsteen PNA strand is responsible for the significant increase in T_{ass} at pH 5.5 for homopyrimidine PNAs. The $\Delta T_{ass}/C^+$ values (Table 2) enabled us to evaluate the effect of protonation per one cytosine in Hoogsteen PNA strand. The data showed the effect of protonation was much higher for PNA 2 without positively charged *lysine* than for PNA 4 and 5 with

lysines. At pH 7.0, antiparallel orientation of PNA 4 and 5 to DNA targets was preferable compared to parallel one. Protonation of cytosines affected triplexes with parallel PNAs twice as much as triplexes with antiparallel PNAs judging by $\Delta T_{ass}/C^+$ values. As a result, at pH 5.5, T_{ass} became similar suggesting there was no preferable binding orientation for positively charged H-PNA strands toward DNA target. Since it is not clear which PNA strand binds tighter to the DNA target under these conditions, it is difficult to assign the peaks in melting curves (Fig. 3a, b) to Hoogsteen or Watson–Crick PNA strand dissociation.

In conclusion, we have shown that T_{ass} values for PNA_2–DNA triplex formation derived from nonequilibrium reassociation curves correlated well with log K_{50} derived from equilibrium mobility shift experiments. The correlation obtained enabled evaluation of affinity of single and bis pyrimidine PNAs which bind slowly single stranded DNA/RNA targets using fast and convenient UV absorption method.

ACKNOWLEDGEMENTS

We thank Dr Richard Friedman for very useful discussion, Dr Alexander Vologodsky for critical reading of the manuscript, and Dr Rolf Berg for synthesis of some of the PNAs.

REFERENCES

1 Nielsen, P. E., Egholm, M., Berg, R. H. and Buchardt, O. (1991) *Science*, **254,** 1497–1500.
2 Egholm, M., Buchardt, O., Nielsen, P. E. and Berg, R. H. (1992) *J. Am. Chem. Soc*., **114,** 1895–1897.
3 Kim, S. K., Nielsen, P. E., Egholm, M., Buchardt, O., Berg, R. H. and Norden, B. (1993) *J. Am. Chem. Soc*., **115,** 6477–6481.
4 Egholm, M., Buchardt, O., Christensen, L., Behrens, C., Freier, S. M., Driver, D. A., Berg, R. H., Kim, S. K., Norden, B. and Nielsen, P. E. (1993) *Nature*, **365,** 566–568.
5 Griffith, M. C., Risen, L. M., Greig, M. J., Lesnik, E. A., Sprankle, K., Griffey, R., Kiely, J. S. and Freier, S. M. (1995) *J. Am. Chem. Soc*., **117,** 831–832.
6 Bonham, M. A., Brown, S., Boyd, A. L., Brown, P. H., Bruckenstein, D. A., Hanvey, J. C., Thomson, S. A., Pipe, A., Hassman, F., Bisi, J. E., Froehler, B. C., Matteucci, M. D., Wagner, R. W., Noble, S. A. and Babiss, L. E. (1995) *Nucleic Acids Res*., **23,** 1197–1203.
7 Noble, S. A., Bonham, M. A., Bisi, J. E., Bruckenstein, D. A., Brown, P. H., Brown, S. C., Cadilla, R., Gaul, M. D., Hanvey, J. C., Hassman, C. F., Josey, J. A., Luzzio, M. J., Myers, P. M., Pipe, A. J., Ricca, D. J., Su, C. W., Stevenson, C. L., Thomson, S. A., Wiethe, R. W. and Babiss, L. E. (1995) *Drug Dev.Res*., **34,** 184–195.
8 Egholm, M., Christensen, L., Dueholm, K. L., Buchardt, O., Coull, J. and Nielsen, P. E. (1995) *Nucleic Acids Res*., **23,** 217–222.
9 Pyle, A. M., McSwiggen, J. A. and Cech, T. R. (1990) *Proc. Natl. Acad. Sci. USA*, **87,** 8187–8191.
10 Shindo, H., Torigoe, H. and Sarai, A. (1993) *Biochemistry*, **32,** 8963–8969.
11 Lima, W. F., Monia, B. P., Ecker, D. J. and Freier, S. M. (1992) *Biochemistry*, **31,** 12055–12061.
12 Ecker, D. J., Vickers, T. A., Bruice, T. W., Freier, S. M., Jenison, R. D., Manoharan, M. and Zounes, M. (1992) *Science*, **257,** 958–961.
13 Kawasaki, A. M., Casper, M. D., Freier, S. M., Lesnik, E. A., Zounes, M. C., Cummins, L. L., Gonzalez, C. and Cook, P. D. (1993) *J. Med. Chem*., **36,** 831–841.
14 Laggriffoul, P.-H., Egholm, M., Nielsen, P. E., Berg, R. H. and Buchardt, O. (1994) *Bioorg. Med. Chem. Lett*., **4,** 1081–1082.
15 Fried, M. and Crothers, D. M. (1981) *Nucleic Acids Res*., **9,** 6505–6525.
16 Garner, M. M. and Revzin, A. (1981) *Nucleic Acids Res*., **9,** 3047–3060.
17 Wyatt, J. R., Davis, P. W. and Freier, S. M. (1996) *Biochemistry*, **35,** 8002–8008.
18 Anshelevich, V. V., Vologodskii, A. V., Lukashin, A. V. and Frank-Kamenetskii, M. D. (1984) *Biopolymers*, **23,** 39–58.
19 Demidov, V. V., Yavnilovich, M. V., Belotserkovskii, B. P., Frank-Kamenetskii, M. D. and Nielsen, P. E. (1995) *Proc. Natl. Acad. Sci. USA*, **92,** 2637–2641.
20 Almarsson, O. and Bruice, T. C. (1993) *Proc. Natl. Acad. Sci. USA*, **90,** 9542–9546.
21 Il′icheva, I. A., Terekhova, E. V., Tsybenko, S. Y., Kunitzin, A. G. and Florentiev, V. L. (1994) *Int. J. Quantum Chem., Quantum Biol. Symp*., **21,** 157–172.
22 Betts, L., Josey, J. A., Veal, J. M. and Jordan, S. R. (1995) *Science*, **270,** 1838–1841.
23 Rougee, M., Faucon, B., Mergny, J. L., Barcelo, F., Giovannangeli, C., Garestier, T. and Helene, C. (1992) *Biochemistry*, **31,** 9269–9278.
24 Lavelle, L. and Fresco, J. R. (1995) *Nucleic Acids Research*, **23,** 2692–2705.
25 Rose, D. J. (1993) *Anal.Chem*., **65,** 3545–3549.